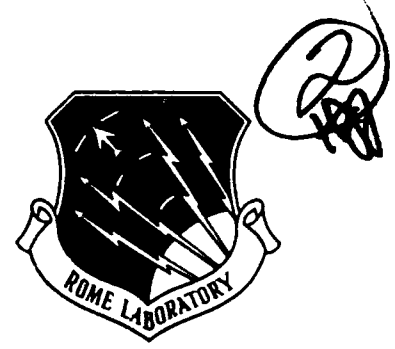


AD-A267 721



RL-TR-93-58
Final Technical Report
May 1993

OPTICAL RESIDUE PROCESSING MODULE

BDM International, Inc.

**Michael W. Haney, James J. Levy (BDM International, Inc.);
Ravindra A. Athale, Gary W. Euliss (George Mason University)**

APPROVED FOR PUBLIC RELEASE; DISTRIBUTION UNLIMITED.

420
473
93-18330

DTIC
ELECTE
AUG 10 1993
S B D

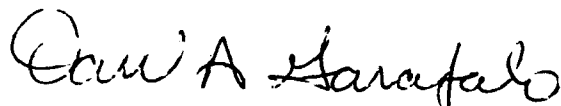
Rome Laboratory
Air Force Materiel Command
Griffiss Air Force Base, New York



This report has been reviewed by the Rome Laboratory Public Affairs Office (PA) and is releasable to the National Technical Information Service (NTIS). At NTIS it will be releasable to the general public, including foreign nations.

RL-TR-93-58 has been reviewed and is approved for publication.

APPROVED:



DAVID A. GARAFALO
Project Engineer

FOR THE COMMANDER:



JOHN A. GRANIERO
Chief Scientist
Command, Control, and Communications Directorate

If your address has changed or if you wish to be removed from the Rome Laboratory mailing list, or if the addressee is no longer employed by your organization, please notify RL (C3DB) Griffiss AFB NY 13441-5700. This will assist us in maintaining a current mailing list.

Do not return copies of this report unless contractual obligations or notices on a specific document require that it be returned.

REPORT DOCUMENTATION PAGE

Form Approved
OMB No. 0704-0188

Public reporting burden for this collection of information is estimated to average 1 hour per response, including the time for reviewing instructions, searching existing data sources, gathering and maintaining the data needed, and completing and reviewing the collection of information. Send comments regarding this burden estimate or any other aspect of this collection of information, including suggestions for reducing this burden, to Washington Headquarters Services, Directorate for Information Operations and Reports, 1215 Jefferson Davis Highway, Suite 1204, Arlington, VA 22202-4302, and to the Office of Management and Budget, Paperwork Reduction Project (0704-0188), Washington, DC 20503.

1. AGENCY USE ONLY (Leave Blank)		2. REPORT DATE May 1993	3. REPORT TYPE AND DATES COVERED Final Jul 91 - Dec 92	
4. TITLE AND SUBTITLE OPTICAL RESIDUE PROCESSING MODULE			5. FUNDING NUMBERS C: F30602-91-C-0052 PE: 63726F PR: 2863 TA: 92 WU: PQ	
6. AUTHOR(S) Michael W. Haney, James J. Levy (BDM International, Inc.) Ravindra A. Athale, Gary W. Euliss (George Mason University)				
7. PERFORMING ORGANIZATION NAME(S) AND ADDRESS(ES) BDM International, Inc. 7915 Jones Branch Drive McLean VA 22102-3396			8. PERFORMING ORGANIZATION REPORT NUMBER	
9. SPONSORING/MONITORING AGENCY NAME(S) AND ADDRESS(ES) Rome Laboratory (C3DB) 525 Brocks Road Griffiss AFB NY 13441-4505			10. SPONSORING/MONITORING AGENCY REPORT NUMBER RL-TR-93-58	
11. SUPPLEMENTARY NOTES Rome Laboratory Project Engineer: David A. Garafalo/C3DB (315) 330-7142				
12a. DISTRIBUTION/AVAILABILITY STATEMENT Approved for public release; distribution unlimited.			12b. DISTRIBUTION CODE	
13. ABSTRACT (Maximum 200 words) An experimental program was conducted which demonstrated the Source Modulator Outer Product (SMOP) concept for high speed, high efficiency residue number system (RNS) computation. The optical architecture includes the outer product portion and a mapping portion to implement a Lookup Table (LUT). A Fourier transformbased approach proved better suited to this architecture than did an image-based approach. Also, while the mapping was experimentally performed with optical fibers, a free-space approach based on an array of holographic optical elements is also contemplated. The end product of this research effort included experimental demonstration and a preliminary design of a high performance optical RNS processor based on the SMOP approach.				
14. SUBJECT TERMS Signal Processing, Residue Number System			15. NUMBER OF PAGES 40	
			16. PRICE CODE	
17. SECURITY CLASSIFICATION OF REPORT UNCLASSIFIED	18. SECURITY CLASSIFICATION OF THIS PAGE UNCLASSIFIED	19. SECURITY CLASSIFICATION OF ABSTRACT UNCLASSIFIED	20. LIMITATION OF ABSTRACT U/L	

TABLE OF CONTENTS

Table of Contents	i
List of Figures	iii
I. Program Overview	1
A. Overall Objective	1
B. Statement of Work Summary	1
C. Final Report Chapter Description	2
II. The First Reporting Period	3
A. Moduli and Function Selection	3
B. Two Approaches for the SMOP	4
III. The Second Reporting Period	11
IV. The Third Reporting Period	16
A. Preparation of the Input Fiber Array	16
A. Preparation of the SLM	16
V. The Fourth Reporting Period	18
A. Insertion of the SLM	18
A. Preparation and Insertion of the Output Fiber Mapping	18
VI. The Fifth Reporting Period	21
A. Mapping Efficiency	21
A. Coherent Sources	21
VII. The Sixth Reporting Period	22
A. Mapping Efficiency	22
B. Addition Results	22
VIII. Performance Study and Preliminary Design	25

A.	Performance Study	25
B.	Preliminary Design	27

LIST OF FIGURES

Figure 1.	Experimental setup for implementing the outer product using the Fourier transform method.	7
Figure 2.	CCD image of the outer product plane using the Fourier transform method with incoherent light.	8
Figure 3.	Experimental setup for implementing the outer product using the imaging method.	9
Figure 4.	Actual experimental setup for implementing one dimension of the outer product using the imaging method.	9
Figure 5.	Excerpt of CCD image of the outer product plane using the 1-D imaging method, with two fiber sources as input. The image is the arithmetic difference of two images, one for each fiber, primarily to subtract out dark current noise.	10
Figure 6.	The modulator mask.	13
Figure 7.	Experimental setup for implementing the outer product using the image plane method.	13
Figure 8.	Experimental setup for implementing the outer product using the Fourier plane method.	14
Figure 9.	Input images as they appeared on the modulator mask.	15
Figure 10.	Optical outer-product residue number lookup table schematic.	20
Figure 11.	Mapping from outer-product to residue number output.	20
Figure 12.	Test results for addition of 14 for 10 in a (2, 3, 5) residue system.	23
Figure 13.	Test results for addition of 7 and 2 in a (2, 3, 5) residue system.	23
Figure 14.	Test results for addition of 16 and 9 in a (2, 3, 5) residue system.	24
Figure 15.	Preliminary SMOP design.	29

DTIC QUALITY INSPECTED 3

Accession For	
NTIS GRA&I	<input checked="" type="checkbox"/>
DTIC TAB	<input type="checkbox"/>
Unannounced	<input type="checkbox"/>
Justification	
By _____	
Distribution/	
Availability Codes	
Dist	Avail and/or Special
A-1	

I. PROGRAM OVERVIEW

A. Overall Objective

An experimental program was conducted to demonstrate the Source Modulator Outer Product (SMOP) concept for high speed, high efficiency residue number system (RNS) computation. The SMOP approach, detailed in Appendix B, minimizes power consumption, gate count, and latency in a Lookup Table (LUT) approach that addresses critical mission performance issues in advanced signal processors for spectrum analysis, adaptive radar array null steering, among others. In addition to experiments, analytical studies were carried out on using advanced components for improved performance. The end product of this research effort was an experimental demonstration and a preliminary design of a high performance optical RNS processor based on the SMOP approach.

B. Statement of Work Summary

Task I: Experimental demonstration

A. RNS moduli size selection and function selection:

The sizes of the moduli for the demonstration processor were selected based on available technology and extensibility of the results to a full high performance system. The residue processing function of the experimental module (e.g., multiplication, addition, or quadratic function) was selected to show the advantages of the SMOP approach.

B. Experiments:

The components for the demonstration were selected. Off-the-shelf components were used for the light source, spatial light modulator, and detector array. The table top system were designed for ease of setup and evaluation to facilitate possible demonstrations at other locations.

Task II: Performance capability study

The impact of device (e.g., laser diodes, modulators, hologram arrays) characteristics on the LUT processor performance (e.g., largest modulus, speed, BER) were quantified.

Task III: Preliminary design

A preliminary design of an optical SMOP-based RNS processor for high accuracy, high speed computation was established based on the SMOP architecture's performance capabilities using projected electro-optic technology.

C. Final Report Chapter Description

The original 12-month research program was extended to 18 months through a no-cost extension, to accommodate the efficient scheduling of experiments and analysis at BDM and George Mason University. In the following, the results of each of six reporting periods are reported as separate chapters. Since the focus of this research was on the experimental demonstration of the SMOP concept, the bulk of the results comprise the completion of SOW Task I. B. Tasks II and II were performed in the final month of the program and are reported in the last chapter.

II. THE FIRST REPORTING PERIOD

A. Moduli and Function Selection

Task I. A. was completed with the selection of moduli and function to be demonstrated. The following paragraphs summarize the task results.

The residue number representation requires a set of relatively prime moduli. We evaluated the available components for implementing an experimental version of the SMOP approach, and selected the moduli set of (2,3,5). The dynamic range of a residue system with these moduli is $M = 2 \times 3 \times 5 = 30$. As described below, this moduli set enabled us to evaluate all the key features of the SMOP architecture and project its extensibility to a large dynamic range system.

The SMOP approach generates an outer product image plane; the next issue pertains to the M^2 -to- M mapping. One way to implement this would be to image the M^2 regions of the image plane onto M regions in the next object plane. However, this approach is not general. Holograms, by comparison, could perform any mapping desired. Unfortunately, holograms are generally very sensitive to light input angle; they are also fixed. Optical fibers, on the other hand, can be input coupled and then reassigned with relative ease. As we discovered, however, optical fiber mappers have disadvantages of their own, including poor fan-in and difficulty in fabrication.

A single outer product imaging system can be used to handle more than one modulus. For example, in moduli (2,3,5), a 10×10 outer product architecture ($10 = 2 + 3 + 5$) will suffice. We have decided to use this approach. One input of the outer product consisted of ten LEDs coupled to ten optical fibers, the ends of which were placed in the input plane. This arrangement allowed arbitrary layout of the LEDs with their driver circuitry. The other input started out as a fixed mask, but eventually became a liquid crystal spatial light modulator from an Epson Crystal Image Projector. The SMOP LUT processor had, in its output plane, an array of M^2 optical fiber ends for each modulus M .

For a given function, the system has three independent LUTs. The total number of LUT elements is

$$N = 2^2 + 3^2 + 5^2 = 38.$$

As mentioned above, the three LUTs can be implemented in a single SMOP architecture, in this case using 38 optical fibers to perform the three M^2 -to- M mappings.

The mapping of these M^2 outputs onto M possible inputs depends on exactly what function the LUT is to implement. With this, however, comes the issue of fan-in, in particular the fact that it may vary with LUT. For example, the modulo-5 LUT for the polynomial

$$x^4 + 2x^3y + 3x^2y^2 + 4xy^3 + 5y^4$$

has one one, eight twos, and sixteen threes, resulting in a fan-in of sixteen, not five. In the limit, fan-in can approach the square of the modulus. This fan-in must be achieved without compromising detector speed by increasing its area. With fiber coupling, this may present difficulties. For the purpose of demonstration, we opted to implement the function of addition.

B. Two Approaches for the SMOP

Our goal has been to build the RNS processor using a SMOP approach, followed by a fiber-implemented M^2 -to- M mapping. In the following, we describe two distinct optical methods for implementing the outer product module of the SMOP approach. The purpose of the experimental evaluation during this reporting period was to finalize the approach to be used in the full SMOP demonstration.

Fourier Plane Method

This method is most appropriate for sources and modulators with sizable areas. This is because the 1-D Fourier transform of such an area is a line. The top view of Figure 1 shows the horizontal dimension of this approach. The 30-cm lens takes the

Fourier transform of the input source (one element wide), thus illuminating the entire modulator plane. In the vertical dimension, wherein the source size is a multiple of the modulus, the Fourier transform is a point, coincident with the modulator plane. Beyond the modulator plane is an anamorphic lens combination which has a focal length which in the horizontal direction is half what it is in the vertical direction. (This is achievable by placing a cylindrical lens and spherical lens of equal focal length in close proximity.) Thus the lens combination images in the horizontal dimension, and takes the inverse Fourier transform in the vertical dimension.

Rather than using input LED arrays and real SLMs, our initial experiments simulated these using transparencies. As the top view in Figure 1 shows, the collimated HeNe beam was focused by a cylindrical lens to a vertical line source passing through the first transparency. The entire outer product image was detected by a CCD. We also performed this experiment using incoherent light from a fiber optic lamp. The input cylindrical lens roughly focused this (though not to a line) through the input transparency. Even though true Fourier transforming is not possible with incoherent light, the system did in fact produce an outer product image superior to that achieved with coherent light. This is shown in Figure 2.

Image Plane Method

The image plane method uses a system which magnifies the source plane in one direction and simultaneously demagnifies it in the other. The result is an image whose aspect ratio coincides with the modulators. This modulated image is then magnified in the direction in which it was originally magnified, and 1:1 imaged in the already-magnified direction, onto the outer product plane. This is shown in Figure 3.

Imaging methods suffer the disadvantage that a different lens system should be used for each modulus. Closely related is the fact that, for a given magnification, the modulator size must be proportional to the modulus. Also, if the desired outer product image aspect ratio is 1:1, then the usage of a 1:1 imaging lens with a nonstandard focal length may be required. This is especially true for larger moduli. For example, for modulo 3, a 15-cm f.l. lens whose object is at 20 cm produces a magnified image 60 cm away, as shown in the side view of Figure 3. Since $s + s'$ must also be 80 cm in the

other dimension, a 20-cm f.l. lens must be used. An alternative approach is to allow a rectangular aspect ratio in the outer product plane. So long as $s + s'$ is the same in both dimensions, a crosstalk-free image is obtained in the outer product plane.

To investigate point sources and modulators, we used the setup in Figure 4, which is based upon the side view of Figure 3. The source plane consisted of the ends of two single-mode optical fibers, one of which at a time can be made to emit. The modulator plane was a 50- μm pinhole. Because no refractive elements in the other dimension were used, the cone of light simply spread in that direction. But, as Figure 5 shows, we were indeed successful in imaging both fibers through the pinhole. Assuming a net magnification of 1, we calculated the fiber ends to be about 162 μm apart. When the fibers were translated just outside this range, the pinhole blocked their emitted light. This is consistent with the presence of a 3:1 demagnified image at the 50- μm pinhole.

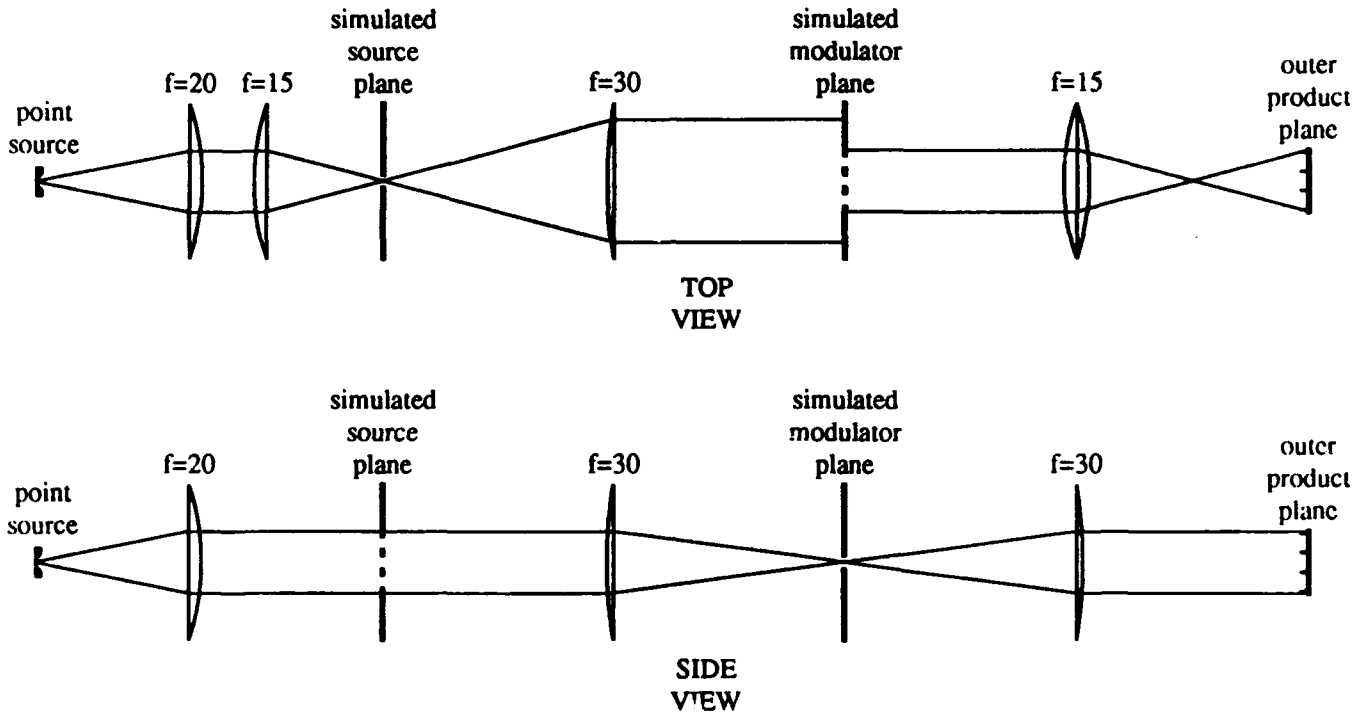


Figure 1. Experimental setup for implementing the outer product using the Fourier transform method.

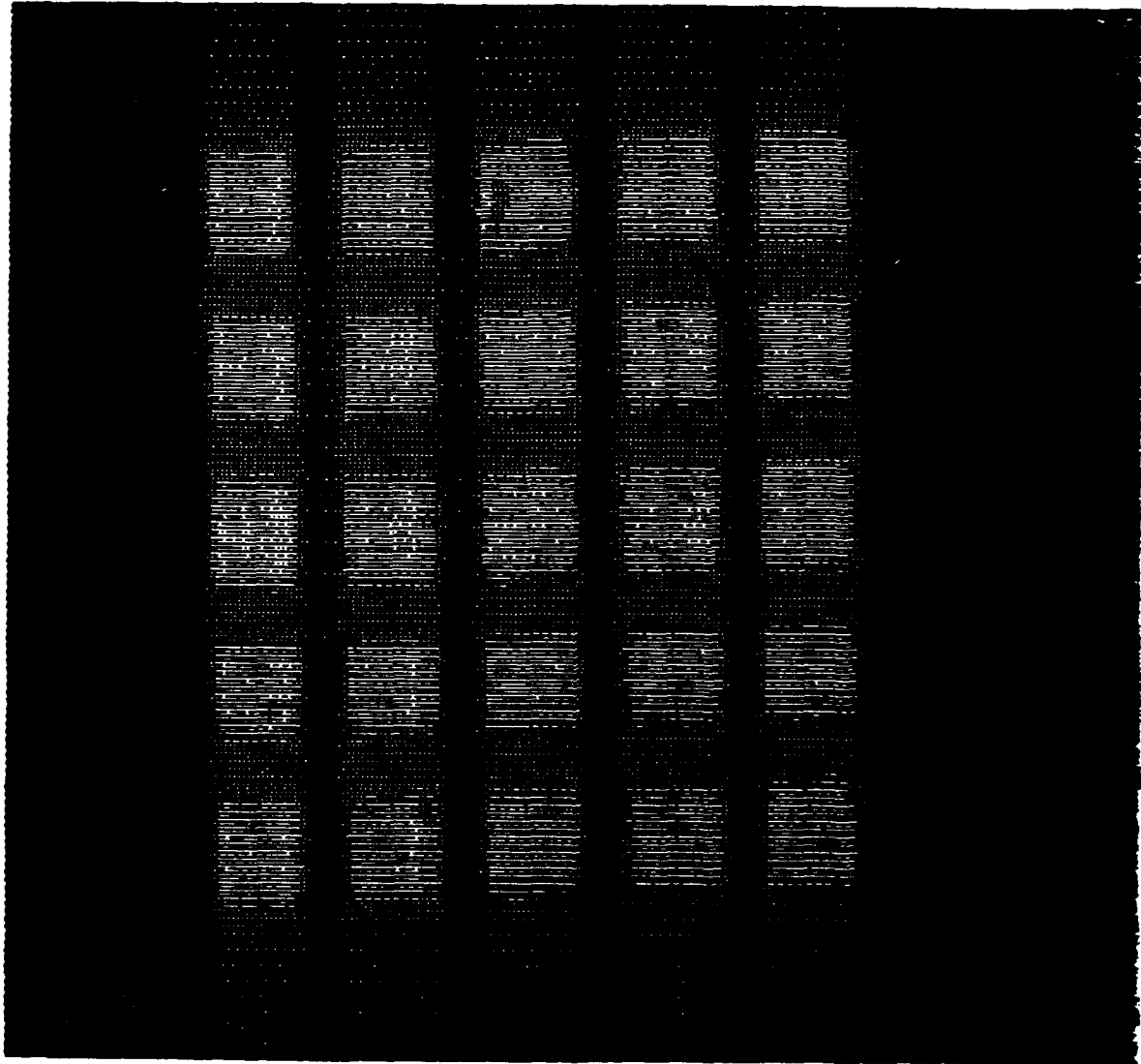


Figure 2. CCD image of the outer product plane using the Fourier transform method with incoherent light.

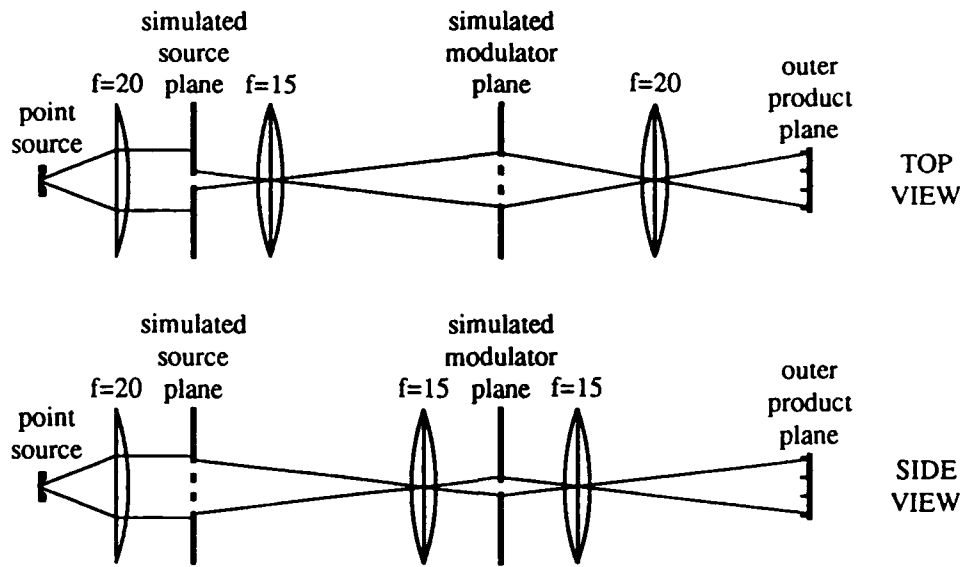


Figure 3. Experimental setup for implementing the outer product using the imaging method.

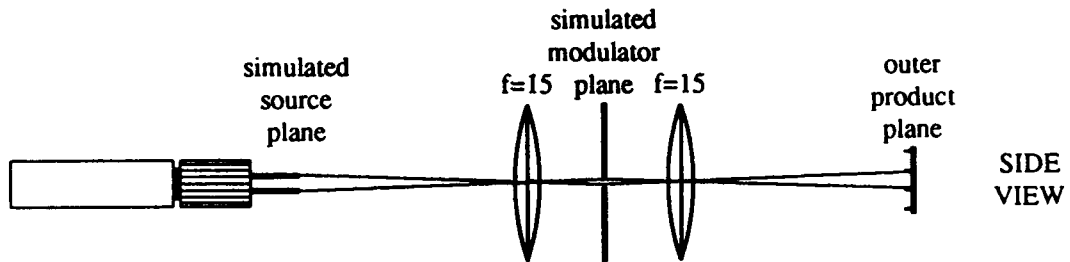


Figure 4. Actual experimental setup for implementing one dimension of the outer product using the imaging method.

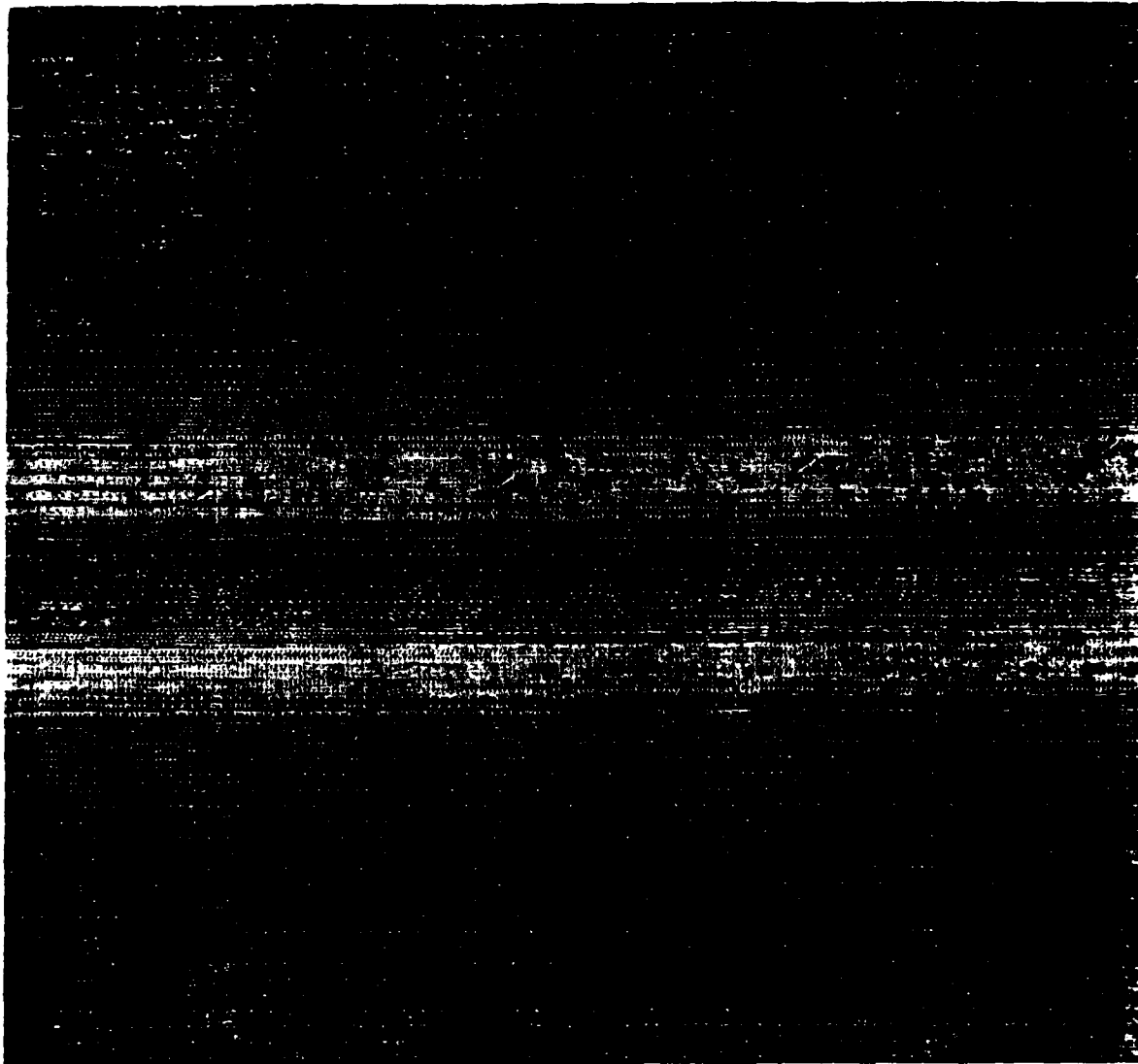


Figure 5. Excerpt of CCD image of the outer product plane using the 1-D imaging method, with two fiber sources as input. The image is the arithmetic difference of two images, one for each fiber, primarily to subtract out dark current noise.

III. THE SECOND REPORTING PERIOD

Our goal was to build the RNS processor using a SMOP approach, followed by a fiber-implemented M^2 -to- M mapping. We experimented further with the two methods described in the last chapter, namely, the image plane and Fourier plane methods. We began by implementing a 10×10 SMOP architecture using incoherent LED inputs. Specifically, a bank of LEDs was pigtailed to 1-mm-diameter plastic optical fibers with smooth end faces and no cladding. The output ends of these fibers were placed in a row in the input plane of the architecture of interest. This approach allowed us to conveniently simulate a row of broadly-emitting, incoherent sources. Indeed, the fibers produced beams having a large spread angle of about 45° . The "modulator" of the SMOP in these experiments consisted of the transparency shown in Figure 6.

Image Plane Method

This method, described in the last chapter, is characterized by a cascade of magnifying/demagnifying astigmatic imaging systems with dimensions specific to the required magnifications, hence, dependent on the modulus (or sum of moduli). Figure 7 shows the layout of the method. A CCD, used for evaluation purposes, is shown in the outer product plane. However, the ultimate implementation will have input fiber ends, for the M^2 -to- M mapping.

Despite its ability to produce sharp outer product images, the imaging method has limited utility. For a given input plane size, the modulator minimum size must be proportional to the modulus. Also, lens f_O must have a nonstandard focal length to produce a square outer product image. For divergent sources such as the 1-mm fiber ends, a great loss of light occurs, because the image of the input LEDs must be demagnified in the row dimension, requiring great distance between object and imaging lens. Short focal lengths can counter this, but for the above-mentioned fibers, with moduli 10 or larger, f_M approaches $1/m$ of the lens diameter. (For example, if the lens diameter is 2", we must have s_L equal 2" and s_S at 0.2"; and so f_M approaches 0.2".)

Fourier Plane Method

This method is more appropriate for sources and modulators which have extended areas. This is because the 1-D Fourier transform of such an area is a line. (Ideally, the source should appear as a broken line.) Figure 8 shows this approach. The first lens takes the Fourier transform in both directions, yielding, at the modulator, a line orthogonal to that of the inputs. Beyond the modulator plane is an anamorphic lens combination which has a focal length which in the horizontal direction is half what it is in the vertical direction. (This is achievable by placing a cylindrical lens and spherical lens of equal focal length in close proximity.) Thus the lens combination images in one dimension, and takes the inverse Fourier transform in the other.

Incidentally, if the sources are area sources, a glass rod parallel to them may be used to produce a broken line source. From there, the Fourier plane method operates.

The method we focused on in the second quarter amounted to a "customized" Fourier approach. Light efficiency becomes the primary concern in a system whose sources are broadly spreading beams from 1-mm plastic fibers.

The first lens, with a focal length of 10 cm, performs in almost the same role as in the Fourier plane method. However, because the sources are divergent in both directions, the modulator is illuminated with m nearly overlapping circles, approximately the diameter of the lens. The observed appearance of the fiber images upon the modulator mask is shown in Figure 9. The circles take on sharp edges, owing to the lens edges; the source divergence is that much.

What made the approach "customized" was that the distance between the input lens and the mask was reduced as necessary to maximize light throughput.

Beyond the mask, our experiment closely resembled the true Fourier plane method. In the horizontal dimension was performed the inverse Fourier transform, using a 15-cm lens; in the vertical direction, two adjacent 15-cm lenses combined to have a 7.5-cm focal length, thus imaging the mask onto the CCD.

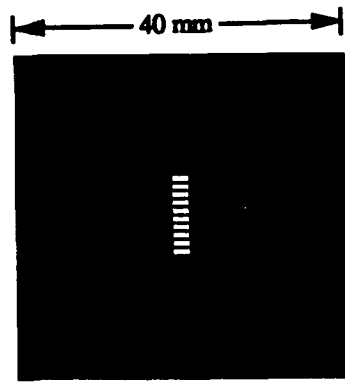


Figure 6. The modulator mask.

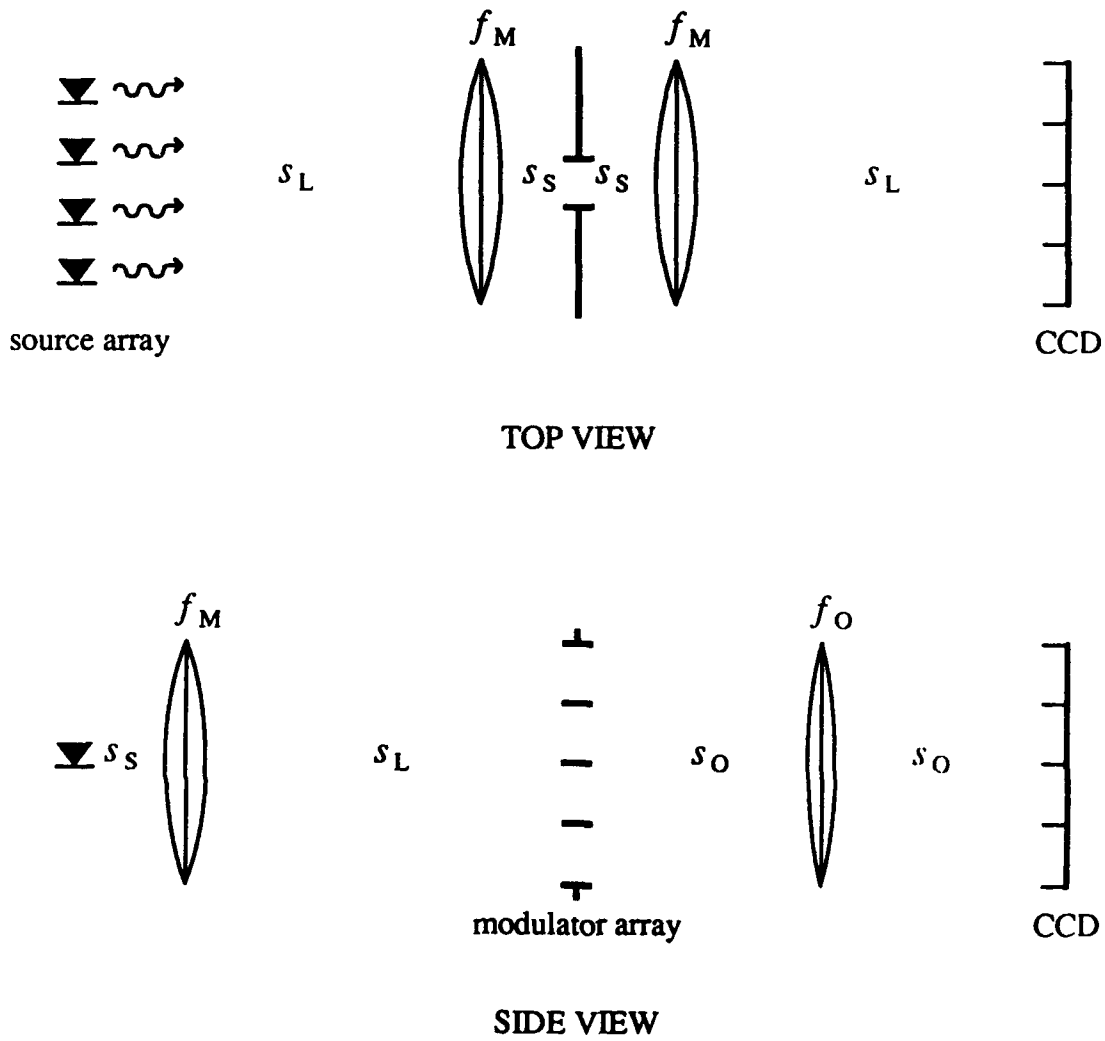
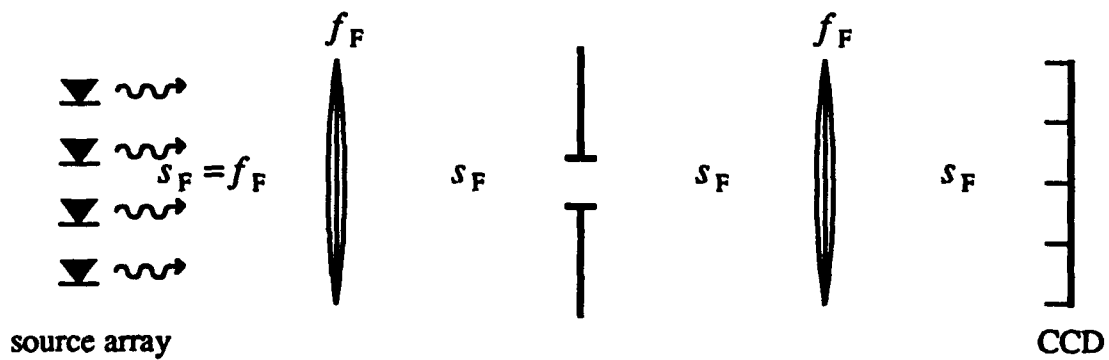
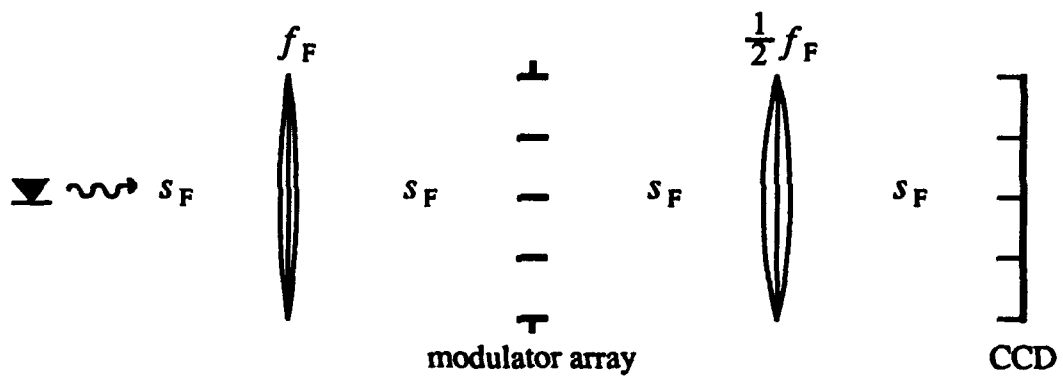


Figure 7. Experimental setup for implementing the outer product using the image plane method.



TOP VIEW



SIDE VIEW

Figure 8. Experimental setup for implementing the outer product using the Fourier plane method.

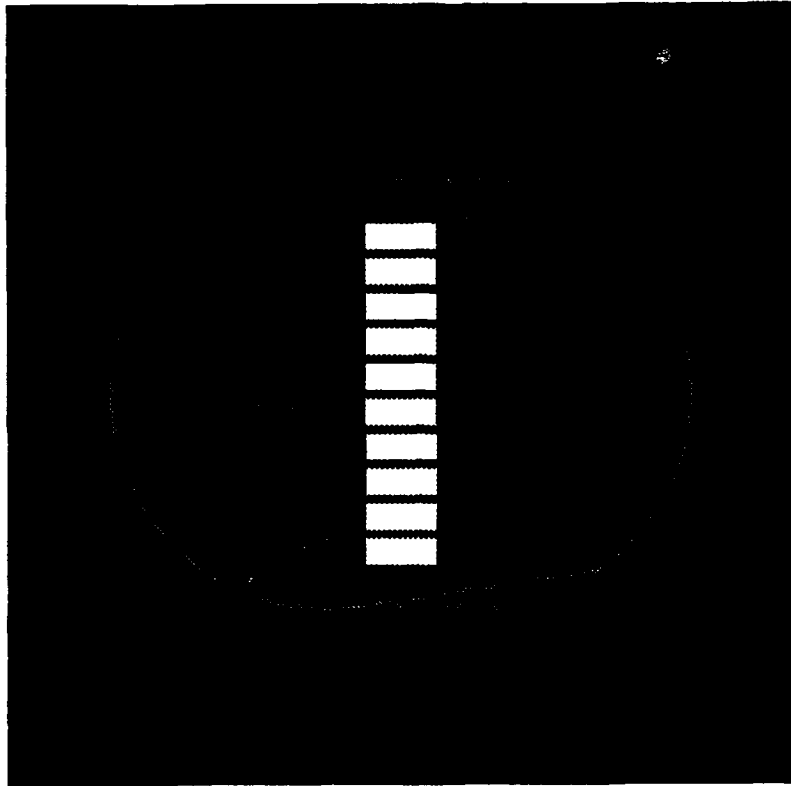


Figure 9. Input images as they appeared on the modulator mask.

IV. THE THIRD REPORTING PERIOD

A. Preparation of the Input Fiber Array

In the third reporting period, work progressed on a 10×10 outer product optical system comprising the first stage of the optical residue processor. Efforts during this reporting period focused on building a 10-element LED array to provide the optical input to the system and setting up the optical system using a fixed 10-element mask. Preparation was made for replacing the fixed mask with a spatial light modulator.

Input to the first stage of the residue processor was supplied by a 10-element LED array. The array was constructed with Motorola model MFOE76 visible LEDs operating at 660 nm. The drive circuit for the array was designed so that any combination of LEDs can be illuminated. Each LED was coupled to a segment of polymethyl methacrylate multimode optical fiber with an outside fiber diameter of 1 mm and an outside jacket diameter of about 2 mm. The fibers are clamped side-by-side with a resulting center-to-center spacing of approximately 2 mm. In order to improve the coupling efficiency and the uniformity across the array the fiber terminations were coarsely polished in a three-step procedure using 32-micron, 15-micron, and 3-micron lapping films.

The fiber array was oriented horizontally in the optical system. Light from the array was collected and roughly collimated by a horizontally mounted 80-mm cylindrical lens. The array was then demagnified in the horizontal axis by a 150-mm cylindrical lens and passed through a mask consisting of 10 4-mm \times 1-mm elements spaced 2 mm center-to-center in a vertical configuration. The output from the mask was then imaged on a CCD camera. The result was a fully populated 10×10 matrix imaged on the CCD.

B. Preparation of the SLM

The SLM that replaced the fixed mask was extracted from an Epson Crystal Image projector system. The projector contains three SLMs, one corresponding to each of the three principle white light components. The three SLMs are functionally identical and contain no color filters, thus allowing their full pixel resolution to be used. Each

SLM area comprises 320×220 pixels. However, depending on the video source, a subset of that area will actually be used. The SLMs are 1.27 inches on the diagonal and are thin film transistors on a quartz substrate with a twisted nematic liquid crystal, operating on the polarization rotation principle. A polarizing film mounted on one side of each SLM has been removed so that an external polarizer/analyzer is needed. The pixel layout is on a rectangular grid and, through preliminary tests, the pixels appeared to be reasonably square.

The existing hardware in the Crystal Image projector was used to drive the SLM. It can accept video input from three different sources: composite video, RGB+sync, and CGA digital signals. The CGA input is the most useful since the CGA medium resolution graphics mode is 320×200 pixels and the control circuitry in the Crystal Image projector is able to map the CGA display region pixel-for-pixel onto the SLM (20 rows of pixels are not used, roughly 10 at the top and 10 at the bottom).

At this point, one SLM was successfully removed from the projector and the necessary connectors and cable were configured so that the device can be externally operated on an optical bench. The necessary interface was established to allow the SLM to be addressed by a desktop computer.

V. THE FOURTH REPORTING PERIOD

A. Insertion of the SLM

During the fourth reporting period, we succeeded in replacing the fixed mask in the intermediate image plane of the processor with the Epson spatial light modulator (SLM) as planned. The vector representation on the SLM consisted of ten elements approximately 0.5 mm wide and 1 cm long spaced 1 mm center-to-center. Horizontal demagnification of the LED array image on the SLM was adjusted so that the size was also approximately 1 cm, resulting in a 1-cm \times 1-cm outer-product pattern between the LED array and the SLM. This allowed the two cylindrical lenses previously used in the output to be replaced by a single spherical lens to produce a magnified outer-product image.

B. Preparation and Insertion of the Output Fiber Mapping

Additional progress was made in the output stage of the processor. Specifically, mapping from the 10 \times 10 outer product to a 10-element vector was achieved using a two-dimensional optical fiber array. A schematic of the optical system with this mapping scheme in place is shown in Figure 10. Reviewing the first stage of the processor, the fiber array was oriented in the horizontal plane in the optical system. Light from the array was collected and collimated by a horizontally mounted 40-mm cylindrical lens. The array was then demagnified and imaged in the horizontal axis by a 150-mm cylindrical lens onto an SLM. The SLM was used to represent a second 10-element vector oriented in the vertical plane. The plane of the SLM was then imaged using a 150-mm spherical lens. The result was a 10 \times 10 vector outer-product matrix in the image plane which contains the 2 \times 2, 3 \times 3, and 5 \times 5 diagonal blocks corresponding to the modulo 2, modulo 3 and modulo 5 residue lookup tables. The output in this plane was mapped into a 10-element vector to provide a representation of the output in the RNS as illustrated in Figure 11. The mapping was accomplished by placing a fiber face plate in the outer-product image plane with a one-to-one correspondence between each element of the lookup table and a fiber termination. The other ends of the fibers were directed to a position corresponding to the appropriate

representation in the output vector. The specific mapping depends on the operation to be performed.

We reported our experimental setup and some results in an oral paper at the 1992 SPIE Aerospace Ser ing Symposium held in Orlando (paper 1703-53), included in Appendix A. The presentation included a videotaped demonstration of the processor. The manuscript was submitted to SPIE Proceedings.

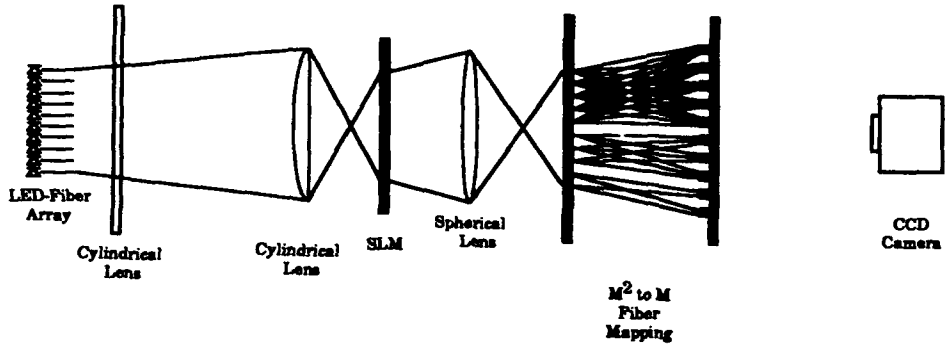


Figure 10. Optical outer-product residue number lookup table schematic.

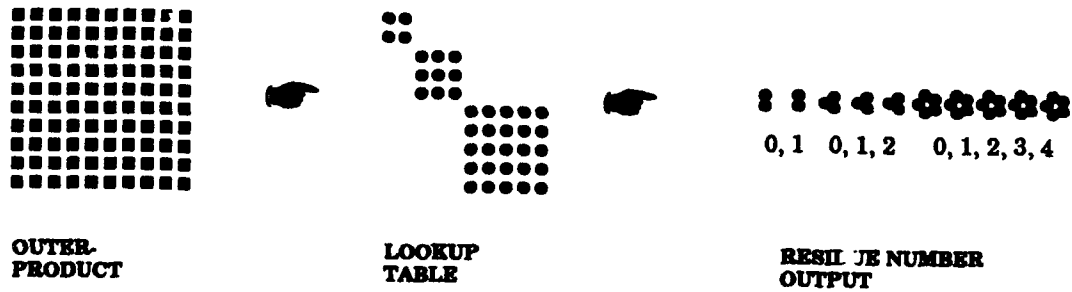


Figure 11. Mapping from outer-product to residue number output.

VI. THE FIFTH REPORTING PERIOD

A. Mapping Efficiency

Efforts during the fifth reporting period were primarily concentrated on improving the transmission efficiency of the system. In the previous results, little effort had been made to maximize the coupling efficiency and transmission quality of the M^2 -to- M fiber mapping device. We made attempts to improve these conditions. Both of the fiber faceplates which produce the mapping were carefully polished in two steps using a 32-micron lapping film followed by a 15-micron lapping film. This is a process similar to that reported for improving the efficiency at the input stage of the processor.

B. Coherent Sources

We also began exploring the use of independently coherent and collimated optical sources for input to the processor. It is desirable to minimize the size of the SLM in the processor design in order to maximize the speed. One factor impeding this is the extent of the image of the optical array when demagnified onto the SLM. The use of laser diodes and gradient-index (GRIN) rods or a lenslet array to individually collimate the light from each diode will allow greater demagnification.

VII. THE SIXTH REPORTING PERIOD

A. Mapping Efficiency

Both ends of the fibers in the M^2 -to- M mapping of the processor were polished to gain some improvement in the coupling efficiency of light into the fibers and the uniformity in the output, so that the overall efficiency of the setup could be improved. It is apparent that in the uncollimated LED/fiber array configuration, a significant amount of power is lost to simple beam divergence. However, in spite of the relatively poor efficiency in this configuration, a sufficient amount of light was transmitted through the system for clear detection at the output end of the M^2 -to- M mapping by a detector array.

B. Addition Results

The results of addition in a (2, 3, 5) residue system are shown in Figures 12-14. Correct results were computed in each case given a proper threshold. A visible problem in the results was that some crosstalk occurred between adjacent channels. This is most apparent in the (16+9) example of Figure 14. The problem was most likely due to the imaging quality of the setup which may have been insufficient to allow absolute separation of the input elements. Increasing the physical separation of the elements in the input source array could improve this condition. However, replacement of the incoherent LEDs coherent laser diodes could also improve the imaging quality.

A second setup was constructed for performing modulo 7 addition. The other primary alteration was that the input array was demagnified by a factor of five at the modulator plane. In addition, a fixed mask was used in the modulator plane. Extreme care was taken to maximize the optical efficiency throughout the system. The power was then measured at several locations along the system in order evaluate the power loss characteristics. To summarize, the efficiency at the back side of the modulator mask was approximately 3×10^{-4} while the overall efficiency was about 10^{-5} .

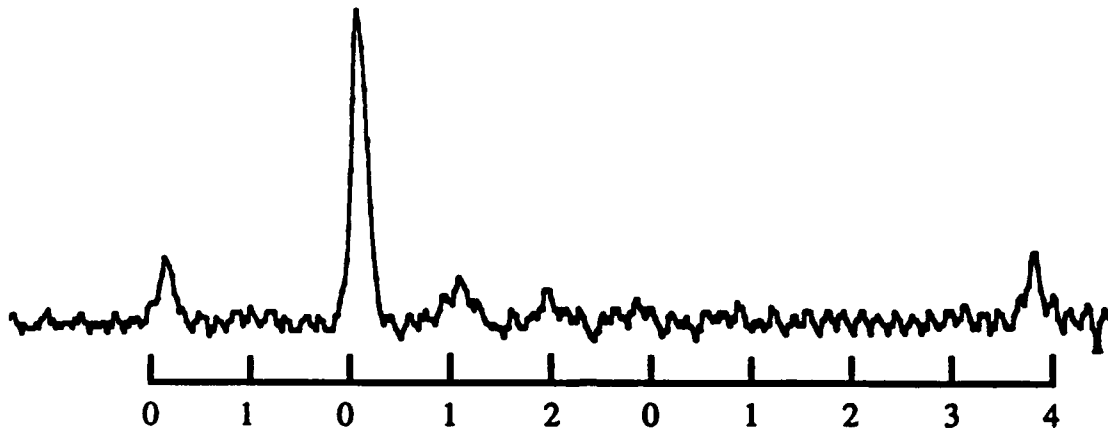


Figure 12. Test results for addition of 14 for 10 in a (2, 3, 5) residue system.
 $14 + 10 = (0,2,4) + (0,1,0) = (0, 0, 4)$

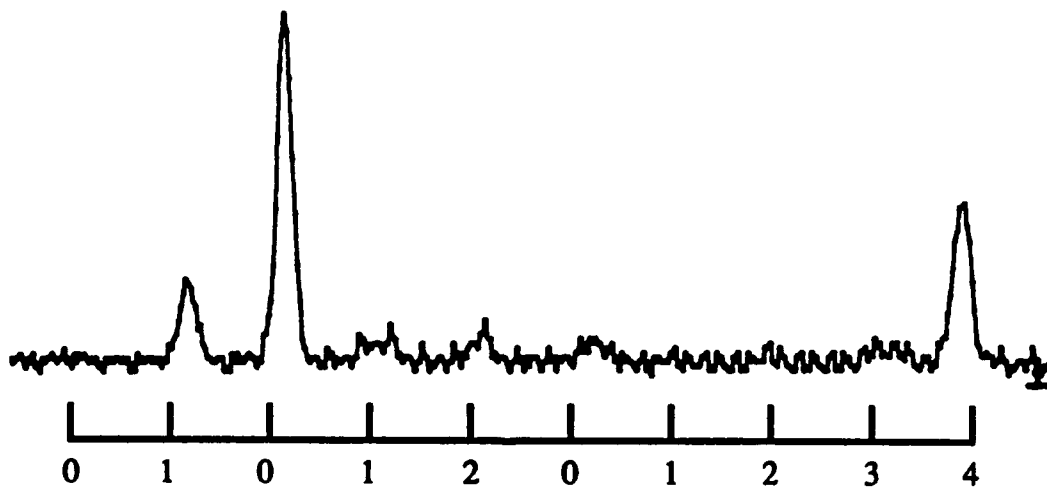


Figure 13. Test results for addition of 7 and 2 in a (2, 3, 5) residue system.
 $7 + 2 = (1,1,2) + (0,2,2) = (1,0,4)$

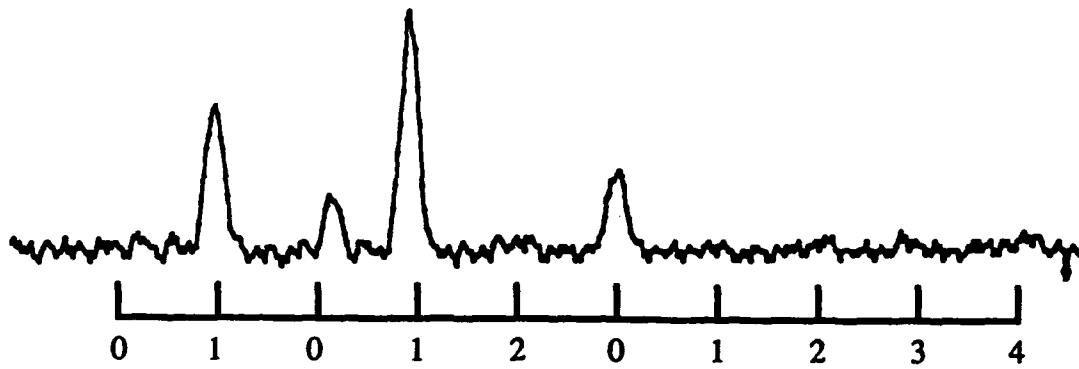


Figure 14. Test results for addition of 16 and 9 in a (2, 3, 5) residue system.
 $16 + 9 = (0,1,1) + (1,0,4) = (1,1,0)$

VII. PERFORMANCE STUDY AND PRELIMINARY DESIGN

The treatment of Tasks II and III was influenced by the following performance goals:

- 1) A system dynamic range of 64 bits requiring a maximum modulus of 47; and
- 2) An operating bandwidth of at least 1 GHz.

Less quantified goals included high optical efficiency, low bit-error rate (BER) or large signal-to-noise ratio, and compact size. The basic selection of optical and optoelectronic devices has direct impact on the ability to achieve these goals. A discussion of the device options is presented below. The recommended choices are then presented in the preliminary SMOP design.

A. Performance Study

The primary devices for consideration can be categorized as the sources, the modulators, the detectors, and the device used to achieve the M^2 -to- M mapping. Let us begin the discussion with the sources. Our options include light-emitting diodes (LEDs) and laser diodes (LDs) and the choice can have an impact on bandwidth, optical efficiency, BER, and size. The important difference between LEDs and LDs is coherence; LEDs are incoherent while LDs are coherent. Coherence of the sources allows for the possibility to obtain diffraction limited (or at least near diffraction limited) performance from the optical elements in the system. This translates to smaller (and hence higher-speed) modulators, a shorter optical system, and better system efficiency than an equivalent incoherent design.

Another difference between the two optional sources is optical power. Although LEDs with sufficiently high output powers are available, it can be said that LDs typically produce more optical power than LEDs. This combined with the superior optical system efficiency will result in higher signal-to-noise ratio and thus lower BER.

One way in which optical modulators can be characterized is by their modulation bandwidth, which is particularly relevant for this discussion. Options that exist include electro-optic modulators, including the liquid crystal-based type, acousto-optic modulators, and quantum well devices. Electro-optic modulators suffer a strong dependence of speed on size. In particular, liquid crystal modulators are simply slow, on the order of kHz. As for acousto-optic modulators (Bragg cells), the necessary technique would be to apply a long waveform whose attenuation history represents in time the desired ON-OFF distribution in space. At a propagation velocity of 0.62×10^3 m/s and assuming a length of about 1 cm, it would take 16 μ s for this waveform to reach its position, resulting in a maximum rate of 62 kHz. In addition, most Bragg cells have low diffraction efficiency.

Of these options, then, the only choice that can truly offer the required bandwidth in the desired configuration is the quantum well modulator. This type of modulator does offer performance at several GHz, and, within reasonable limits, appears to have a speed independent of element size.

We have considered two options for achieving the M^2 -to- M LUT mapping from the outer-product plane to the detectors. This is basically an optical interconnection problem and both options are based on familiar techniques. One approach, which was demonstrated in Task I, utilizes optical fiber to perform the appropriate mapping. The other technique considered uses a holographic optical element (HOE) to perform the interconnections between the elements in the outer product plane and the detectors. The HOE is an option only if laser diodes are used as the input sources. This component of the SMOP is most likely to have a direct impact on optical efficiency and system size. It is not immediately apparent which approach is superior from the standpoint of optical efficiency. However, it is possible that use of an HOE could produce a more compact system than could a fiber array, due to the high bend radius of the fibers. In addition, a computer-generated HOE interconnect would be more convenient to fabricate and insert, should it be necessary to change the LUT mapping.

The final position in the processor where a speed bottleneck might occur is the detectors; these may also suffer optical efficiency limitations. The fundamental tradeoff between active area, sensitivity, and bandwidth must be considered in choosing detectors

for the output stage of the SMOP. A bandwidth on the order of a gigahertz is well within the capabilities of current detector technology so that the options are not strictly limited by our bandwidth goal. However, it is preferable that the active area of the detector closely match the diffraction limited spot size defined by the output mapping optics, in order to avoid reducing significantly the optical efficiency and thereby increasing the sensitivity requirements.

With these device options and their impact on the SMOP performance in mind, we will now discuss the recommended choices in the context of a preliminary system design in the following section.

B. Preliminary Design

Although much of the work in Task I centered on an imaging approach, the above considerations point to the use of a Fourier plane architecture.

An architecture capable of 64-bit operation could be constructed of the relatively prime moduli 7, 13, 16, 17, 19, 23, 25, 27, 29, 31, 37, 41, 43, and 47. (The product of these is 2×10^{19} .) The preliminary design for the SMOP is illustrated in Figure 15. The figure illustrates for example a modulo 7 processor (i.e., seven optical sources and seven modulators), but the design parameters have been determined for the maximum modulus of 47. The processor utilizes laser diode sources along with quantum well modulators and an anamorphic system of lenses and lenslet arrays.

The optical source is an array of mutually incoherent laser diodes with a center-to-center spacing of $200 \mu\text{m}$. Each diode is assumed to have a vertical angular aperture of about 40° and a horizontal angular aperture of 10° . The laser diode array is followed by a cylindrical lenslet array, and it is this that dictates the $200\text{-}\mu\text{m}$ spacing, a reasonable fabrication limit. Each lenslet in the array has a width of $200 \mu\text{m}$ and a focal length of approximately 1 mm.

Lenses L1, L2, L3, and L4 are all assumed to be $f/1$ lenses with focal lengths of 10 mm, 20 mm, 10 mm, and 20 mm, respectively. As the figure shows, lens L1 vertically collimates the light exiting the input cylindrical lenses. Lens L2 then takes

horizontally the Fourier transform of this light. The modulators, in the Fourier plane of L2 will have a horizontal dimension of $250\ \mu\text{m}$ and a center-to-center spacing of $50\ \mu\text{m}$.

Lens L3 vertically images the entire modulator plane onto the outer product plane. Lens L4 horizontally takes an inverse Fourier transform, and, combined with the terminal lenslet array, effectively imaging the input lenslet array onto the outer product plane.

The lenslet array in front of the outer product plane will have the same dimensions as the previous lenslet array following the input sources.

In the outer product plane of the processor is placed an HOE composed of $m \times m$ individual image holograms. Based upon the operation to be performed, the M^2 -to- M mapping from the LUT to the detectors is performed by the HOE. The overall dimensions of the HOE will be approximately 9.4 mm wide by 2.5 mm high for modulo 47 with each individual hologram measuring $200\ \mu\text{m} \times 50\ \mu\text{m}$. The array of detectors is located 10 mm from the HOE. Each detector is an avalanche photodiode with an active region diameter of $200\ \mu\text{m}$ and a 3-dB cutoff of 1 GHz.

Overall dimensions of the SMOP can be estimated from the above specifications. The length from source to detector will be approximately 80 mm. Minimum height is on the order of 10 mm and the minimum width is on the order of 20 mm. Therefore, excluding the electronics required for the sources, modulators, and detectors, the preliminary SMOP package is estimated to require approximately $16\ \text{cm}^3$.

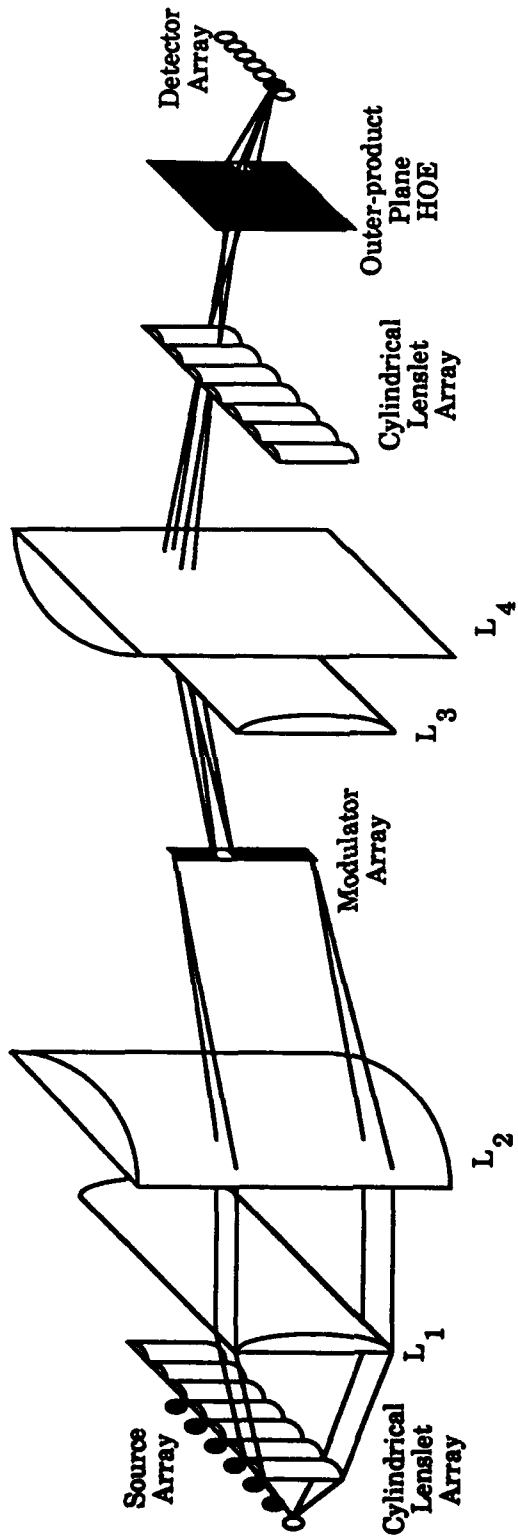


Figure 15. Preliminary SMOP design.

**MISSION
OF
ROME LABORATORY**

Rome Laboratory plans and executes an interdisciplinary program in research, development, test, and technology transition in support of Air Force Command, Control, Communications and Intelligence (C³I) activities for all Air Force platforms. It also executes selected acquisition programs in several areas of expertise. Technical and engineering support within areas of competence is provided to ESD Program Offices (POs) and other ESD elements to perform effective acquisition of C³I systems. In addition, Rome Laboratory's technology supports other AFSC Product Divisions, the Air Force user community, and other DOD and non-DOD agencies. Rome Laboratory maintains technical competence and research programs in areas including, but not limited to, communications, command and control, battle management, intelligence information processing, computational sciences and software producibility, wide area surveillance/sensors, signal processing, solid state sciences, photonics, electromagnetic technology, superconductivity, and electronic reliability/maintainability and testability.